Weierstraß-Institut

für Angewandte Analysis und Stochastik

Leibniz-Institut im Forschungsverbund Berlin e. V.

Light bullets in a time-delay model of a wide-aperture mode-locked semiconductor laser

Alexander Pimenov[1], Julien Javaloyes[2], Svetlana V. Gurevich[3,4],

Andrei G. Vladimirov[1]

submitted: February 5, 2018

[1] Weierstrass Institute
Mohrenstr. 39
10117 Berlin
Germany
E-Mail: alexander.pimenov@wias-berlin.de
andrei.vladimirov@wias-berlin.de

[2] Departament de Física
Universitat de les Illes Balears
C/ Valldemossa km 7.5
07122 Mallorca
Spain
E-Mail: Julien.Javaloyes@uib.es

[3] Institute for Theoretical Physics
University of Münster
Wilhelm-Klemm-Str. 9
48149 Münster
Germany
E-Mail: gurevics@uni-muenster.de

[4] Center for Nonlinear Science (CeNoS)
University of Münster
Corrensstr. 2
48149 Münster
Germany

No. 2481

Berlin 2018

Light bullets in a time-delay model of a wide-aperture mode-locked semiconductor laser

Alexander Pimenov, Julien Javaloyes, Svetlana V. Gurevich, Andrei G. Vladimirov

Abstract

Recently, a mechanism of formation of light bullets (LBs) in wide-aperture passively mode-locked lasers was proposed. The conditions for existence and stability of these bullets, found in the long cavity limit, were studied theoretically under the mean field (MF) approximation using a Haus-type model equation. In this paper we relax the MF approximation and study LB formation in a model of a wide-aperture three section laser with a long diffractive section and short absorber and gain sections. To this end we derive a nonlocal delay-differential equation (NDDE) model and demonstrate by means of numerical simulations that this model supports stable LBs. We observe that the predictions about the regions of existence and stability of the LBs made previously using MF laser models agree well with the results obtained using the NDDE model. Moreover, we demonstrate that the general conclusions based upon the Haus model that regard the robustness of the LBs remain true in the NDDE model valid beyond the MF approximation, when the gain, losses and diffraction per cavity round-trip are not small perturbations anymore.

1 Introduction

Light bullets (LBs) are pulses of electromagnetic energy that are localized both in space and time and preserve their shape in the course of their propagation. Since the paper of Y. Silberberg [1] who coined the term "light bulletsänd demonstrated that the "naive"conservative Kerr LBs found in the Schrödinger equation are unstable and collapse in three dimensions (for more details on the collapse see Refs. [2,3]), experimental observation of LBs remains one of the challenging problems in nonlinear optics. Silberberg showed that the balance between a self-focusing nonlinearity and the spreading effect of chromatic dispersion and/or diffraction was not sufficient to define a robust LB scenario. During the last twenty years, other confinement mechanisms were envisioned in different nonlinear optical systems. In particular, LBs were predicted in dissipative systems like, e.g., optical parametric oscillators [4] or bistable cavities [5, 6] with an instantaneous response of the active medium, and more recently in the output of a passively mode-locked laser operated in the long cavity regime [7, 8]. However, these studies were performed with the help of the Haus-type partial differential equations derived in the mean field (MF) limit when gain and loss per cavity round trip were small and the diffraction was weak, an assumption which is hardly justified for real semiconductor laser devices. Therefore, while the basic mechanism of the formation of the LBs can be qualitatively understood using the models of Refs. [7, 8], determining the parameter domains where this phenomenon can be observed experimentally requires further theoretical studies. To that end, the understanding of the existence and stability properties of LBs with respect to various laser parameters is crucial for the experimental success, which is an ongoing research for the moment.

Unlike the MF laser models, the delay differential equations (DDEs) developed in [9–11] and successfully applied to analyse complex dynamical phenomena in mode-locked lasers [9–13], are free from

the small gain and loss approximation. The DDE model describes time evolution of the slowly varying envelope of the electric field in a ring cavity consisting of multiple sections such as gain, absorber, and spectral filter under some general physical assumptions about each section [10]. Moreover, DDE laser models were successfully tested over recent years to investigate multi-longitudinal-mode regimes observed in various experimental setups [12–18] including the lasers with Fabry-Perot cavities [19–22], which are conventionally studied using more complicated travelling wave partial differential equation models [23–27].

To study the dynamics of a wide aperture mode-locked semiconductor laser we derive a nonlocal delay-differential equation (NDDE) model that can be considered as a generalized version of the DDE mode-locking model taking into account the diffraction in the transverse plane. Using this model we discover for the first time stable LBs in the parameter domain where the MF approximation is no longer valid, and demonstrate that their existence ranges and stability properties are qualitatively similar to those found in [7, 8], which confirms the robustness of the LBs. Furthermore, we demonstrate that by using a spectral method optimized for the computation of LBs in a narrow temporal window we can considerably reduce the LB computation cost. We use the spectral functional mapping to study the stability properties of the LBs in transition away from the MF limit, and show that numerical results obtained using this method are in perfect agreement with those obtained by direct numerical integration of the NDDE model. It is noteworthy that following the approach introduced in [28] in the limit of small gain and loss per cavity round-trip and weak diffraction one can reduce the described NDDE model to generic partial differential MF equations of the Haus type where the effects of gain, losses, chromatic dispersion and/or diffraction can be easily incorporated. On the other hand, incorporating chromatic dispersion into the DDE models is not as straightforward. For example, theoretical approaches allowing to extend DDE models of multimode lasers to account for chromatic dispersion of the intracavity media leading to differential equations with distributed time delay were proposed in [14, 29, 30].

2   Model equations

In this section we derive a model of a wide-aperture mode-locked semiconductor laser shown schematically in Fig. 1. Similarly to [9–11] we use the lumped element approach, which assumes that gain, absorption, diffraction, and spectral filtering are separated and attributed to different laser sections. Therefore, assuming that the absorber and gain sections are very thin and placed one after another, we neglect the diffraction and express the electric field amplitude A_2 on the output of the gain section via the amplitude A_1 on the entrance of the absorber section as:

$$A_2(t, x, y) = e^{(1-i\alpha_g)G(t,x,y)/2 - (1-i\alpha_q)Q(t,x,y)/2 + i\phi_1} A_1(t - t_1, x, y), \tag{1}$$

where t_1 describes small time delay introduced by these two sections, α_g and α_q are linewidth enhancement factors, ϕ_1 is the phase shift, G and Q are the saturable gain and loss proportional to the integrals of the carrier density along the characteristics over the gain and absorber sections, respectively [9–11].

Next, we consider a section where the diffraction takes place. In the Fresnel diffraction approximation the output field A_3 from this section can be expressed via the input field A_2 as follows

$$A_3(t, x, y) = \frac{e^{ikL}}{2\pi i} \int\!\!\!\int_{-\infty}^{\infty} e^{i\left[(x-x')^2 + (y-y')^2\right]/2} A_2(t - t_2, x', y')dx'dy', \tag{2}$$
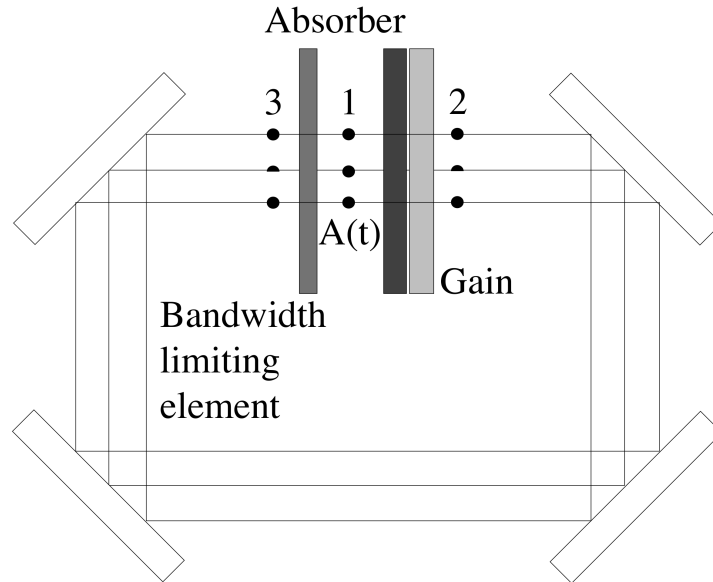
Figure 1: Schematic representation of a wide-aperture ring external cavity laser with thin absorber, gain, and spectral filtering sections. The numbered points 1, 2, and 3 indicate the longitudinal coordinates of the transverse sections where the electric field envelopes A_j with $j = 1, 2, 3$ are evaluated. The relation between these envelopes are given by Eqs. (1)-(3).

where x and y are dimensionless transverse coordinates, L is the section length, $t_2 = L/v$ is the delay time, v is the light velocity, and k is the light wave number in the diffractive section.

Light propagation through the thin spectral filtering section is described by

$$A_4(t, x, y) = \int_{-\infty}^{t} f(t - \theta) A_3(\theta, x, y) d\theta.$$ (3)

In particular, for Lorentzian spectral filter with halfwidth γ and detuning ω_0 we choose $f(t) = \gamma e^{(-\gamma + i\omega_0)t}$.

Finally substituting (1) and (2) into (3), differentiating the resulting equation, setting $\omega_0 = 0$, and using the boundary condition $A_4(t, x, y) = \sqrt{\kappa} A_1(t + T, x, y)$, where κ is the attenuation factor taking into account losses due to output coupling as well as distributed linear losses of the intracavity media, we obtain the following set of NDDEs:

$$\frac{dA}{dt} + \gamma A = \gamma \sqrt{\kappa} \frac{e^{i\phi}}{2\pi i} \int\!\!\int_{-\infty}^{\infty} e^{i\left((x-x')^2 + (y-y')^2\right)/2} \times$$

$$\times e^{(1-i\alpha_g)G/2 - (1-i\alpha_q)Q/2} A(t - T, x', y') dx' dy',$$ (4)

where $A(t, x, y) \equiv A_1(t, x, y)$, T is the total cold cavity round trip time, the propagation factor ikL has been absorbed into the phase ϕ, $\phi = \phi_1 + kL$, and saturable gain G and loss Q fields satisfy the equations [9–11]:

$$\frac{dG}{dt} = \gamma_g(G_0 - G) - (e^G - 1)e^{-Q} |A(t - T, x, y)|^2,$$ (5)

$$\frac{dQ}{dt} = \gamma_q(Q_0 - Q) - s(1 - e^{-Q}) |A(t - T, x, y)|^2.$$ (6)

Here, G_0 (Q_0) is the unsaturated gain (loss) parameter, γ_g (γ_q) is the carrier relaxation rate in the gain (absorber) section, and the parameter s is the ratio of saturation intensities in the gain and absorber sections. In the case of single transverse dimension instead of Eq. (4) we have

$$\frac{dA}{dt} + \gamma A = \gamma\sqrt{\kappa}\frac{e^{i\phi}}{\sqrt{2\pi i}}\int_{-\infty}^{\infty} e^{i(x-x')^2/2}e^{(1-i\alpha_g)G/2-(1-i\alpha_q)Q/2}A(t-T,x')dx'. \qquad (7)$$

NDDE models given by Eqs. (4)-(6) and (5)-(7) can be considered as generalizations of the DDE model introduced in [9–11] to the case when the transverse diffraction of the laser beam is taken into account. In the next sections we use these models for numerical study of LBs in a wide-aperture semiconductor mode-locked laser.

3 Simulations

3.1 Numerical method

For numerical solution of Eqs. (4)-(6) and (5)-(7) we perform Fourier transform (denoted by $\mathcal{F}_\perp$) of Eqs. (4) (or (7)) in the transverse plane

$$\frac{d\tilde{A}}{dt} + \gamma\tilde{A} = \gamma\sqrt{\kappa}e^{-iq^2}\mathcal{F}_\perp\left[e^{(1-i\alpha_g)G/2-(1-i\alpha_q)Q/2+i\phi}A(t-T,x,y)\right], \qquad (8)$$

with $\tilde{A} = \mathcal{F}_\perp[A]$ and $q^2 = q_x^2 + q_y^2$, where q_x and q_y are two components of the normalized transverse wave number. Note that for the sake of convenience in our numerical simulations starting from Eq. (8) we use the rescaled transverse variables $\bar{x} = x\sqrt{2}$ and $\bar{y} = y\sqrt{2}$, with overbar omitted. The numerical method is realised very similarly to the conventional split-step method, so that the systems (4)-(6) and (5)-(7) require as much computational effort as, e.g., 1+1D and 2+1D Ginzburg-Landau-type problems with delay, correspondingly [31–34]. First, using the delayed field $A(t-T,x,y)$ we obtain the values of G and Q on the next step by solving numerically Eqs. (5) and (6). Second, we propagate the Fourier-transformed field $\tilde{A}$ one time step further. Then the procedure is repeated. The large delay does not induce additional computational costs, because we use the values of the field that were calculated in the past. However, it increases significantly the memory requirements. These requirements could be, in principle, relaxed if we use the localized nature of our solution and store the delayed value of the field $A(t-T,x,y)$ only when its absolute value is sufficiently large. Moreover, as it is shown in the following subsection, it is also possible to neglect completely the dynamics outside of a narrow temporal window around a single LB in a similar way as it was done for the MF models discussed in [7].

3.2 Spectral method optimized for single LBs

The field equation given by Eq. (4) can be formally rewritten as

$$\frac{\dot{A}}{\gamma} = -A + \hat{g}\left[A\left(t-T\right)\right], \qquad (9)$$

where $\hat{g}$ is the nonlinear operator that combines the effect of gain, losses, diffraction in Fourier space, and whose expression is given by the right hand side of Eq. (4). Writing Eq. (9) in this particular form makes it apparent that the term $\hat{g}\left[A\left(t-T\right)\right]$ is a known nonlinear function of the field at the previous round trip. One can then solve Eq. (9) for the field profile over a whole round trip that we denote A_n. Several methods are possible, but the most convenient choice is to use the Fourier transform, since transverse diffraction can also be evaluated that way. In particular, the fact that the pulse train is asymptotic to zero makes it possible to apply the Fourier transform along the propagation axis (i.e., in the time domain) with periodic boundary conditions. Solving Eq. (9) in Fourier space and transforming back to the time domain yields a simple expression of the mapping operator

$$A_n = \mathcal{F}_t^{-1}\left\{\mathcal{L}\left(\omega\right)\mathcal{F}_t\left[\hat{g}\left(A_{n-1}\right)\right]\right\}, \tag{10}$$

where $\mathcal{F}_t$ denotes the Fourier transform in time and $\mathcal{L}\left(\omega\right)=\left(1+i\omega/\gamma\right)^{-1}$ is the Lorentzian function. The fact that equations of the same type as Eq. (9) could be solved by a Fourier method as a functional mapping in the long delay limit was already pointed out in [35] for the case of a single variable. Applying Fourier transformation in the transverse plane yields the following form of the functional mapping

$$A_n = \mathcal{F}_t^{-1}\left\{\mathcal{L}\left(\omega\right)\mathcal{F}_t\mathcal{F}_\perp^{-1}\left[e^{-iq^2}\mathcal{F}_\perp\left(e^{(1-i\alpha_g)G_{n-1}/2-(1-i\alpha_q)Q_{n-1}/2+i\phi}A_{n-1}\right)\right]\right\} \tag{11}$$

with the carrier profiles G_{n-1} and Q_{n-1} that can be deduced from the field distribution A_{n-1}. Finally, using the fact that the function $\mathcal{L}\left(\omega\right)\left(e^{-iq^2}\right)$ does not depend on transverse wavenumber q (frequency ω), we can reorder the Fourier transformations to obtain

$$A_n = \mathcal{F}^{-1}\left[\mathcal{U}\left(\omega,q\right)\mathcal{F}\left(e^{(1-i\alpha_g)G_{n-1}/2-(1-i\alpha_q)Q_{n-1}/2+i\phi}A_{n-1}\right)\right] \tag{12}$$

with $\mathcal{F}=\mathcal{F}_t\circ\mathcal{F}_\perp$ and $\mathcal{U}\left(\omega,q\right)=\mathcal{L}\left(\omega\right)e^{-iq^2}\exp\left(iv\omega\right)$, where the last exponential factor represents an ad hoc correction to the natural drift of the temporal solution from one round-trip toward the next. Such drift is found in most DDE systems and in our case, one can simply take $v\approx-1/\gamma$, see [10, 35] for more details.

A numerical method based on the use of Eq. (12) was applied to calculate bifurcation diagrams of the LB solutions. An important advantage of this approach is that the temporal domain along the t-axis can be taken much smaller than the delay time T, e.g. a few times larger than the LB temporal width, yielding a considerable reduction of computational cost.

4 Results

4.1 Light bullets in the mean-field approximation

Self-organization mechanism leading to the formation of LBs in the wide-aperture mode-locked laser is related to the presence of saturable absorption in the laser cavity rather than self-focusing Kerr non-linearity, and one can observe them with zero alpha-factors [7]. Therefore, we start with the simplest case $\alpha_g=\alpha_q=0$ and choose the parameter region, where the gain and loss per cavity round trip are relatively small, so that the MF approximation can be used: $\kappa=0.8$, $Q_0=0.3$, $\gamma_g=0.04$, $\gamma_q=1.0$, $s=30$, $\gamma=40$, $T=200$. We vary the normalized gain $g_0=G_0/g_{th}$, where $g_{th}=Q_0-\log\kappa$, below the lasing threshold $g_0<1$.

A stable two-dimensional LB calculated for $g_0=0.68$ is shown in Fig. 2, while Fig. 3 presents a stable three-dimensional LB obtained for $g_0=0.69$. Note, that the very long tail of the LB that stems from
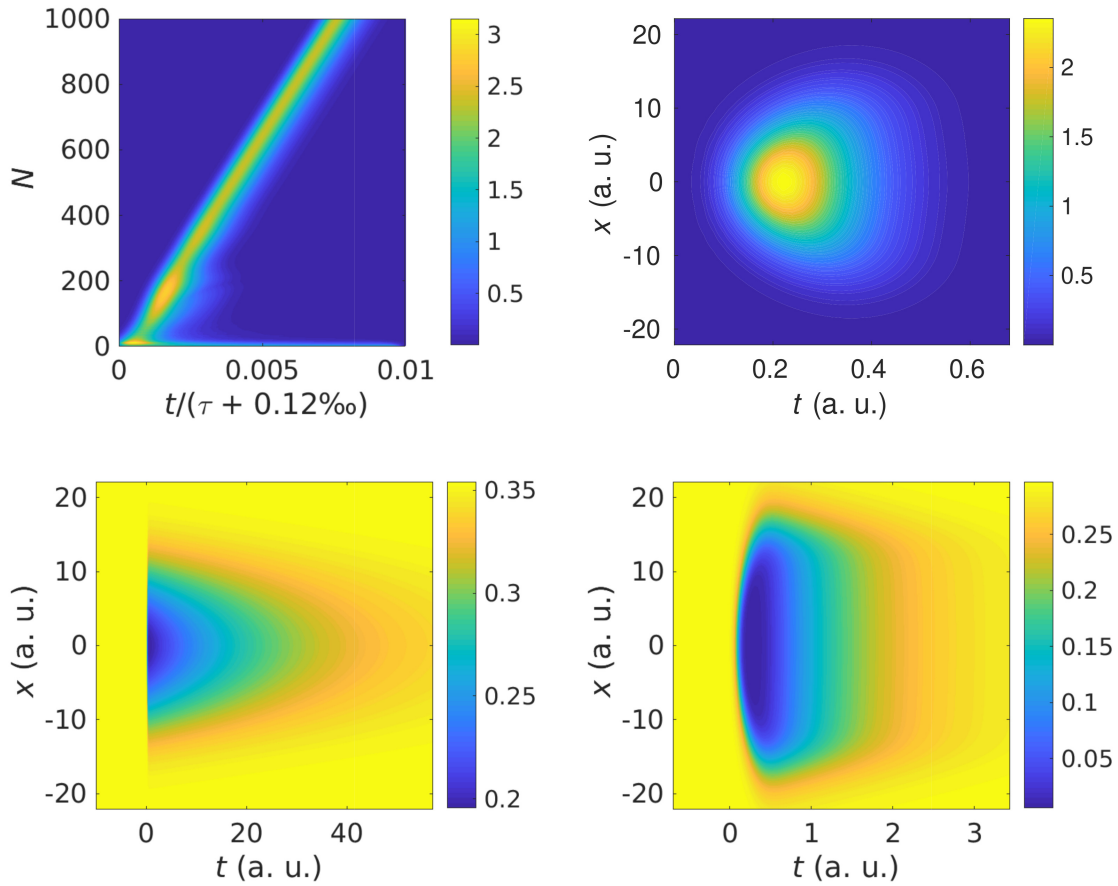
Figure 2: Two-dimensional LB solution obtained by the numerical integration of Eqs. (5)-(7) for $g_0 = 0.68$. Top left panel demonstrates the space-time representation of the maximal intensity $\max_x |A(t,x)|^2$, where N is the number of round-trips adjusted by a multiplication factor 1.00012, which reduces the speed of the LB and improves its visibility in the representation. Top right, bottom left and right panels show spatiotemporal profiles of LB intensity $|A(t,x)|^2$, saturable gain $G(t,x)$, and saturable loss $Q(t,x)$, correspondingly. Other parameters are $\kappa = 0.8$, $Q_0 = 0.3$, $\gamma_g = 0.04$, $\gamma_q = 1.0$, $s = 30$, $\gamma = 40$, $T = 200$, $\alpha_g = \alpha_q = 0$.

the slow gain profile is fully resolved by solving numerically Eqs. (4)-(6) and (5)-(7). Unlike the Haus-type model, which was used earlier in [7] for qualitative modelling of LB regime in the MF limit, these equations give a more realistic description of dynamical behavior of a wide aperture mode-locked semiconductor laser under investigation. Therefore, our results presented in Figs. 2 and 3 provide further arguments in favour of the feasibility of the experimental observation of LBs, predicted in the earlier work of [7].

The domains of the existence of stable two-dimensional LBs obtained by numerical integration of Eqs. (5)-(7) are shown in Fig. 4. The left (right) panel presents the stability domain in the plane of two parameters, pump parameter g_0 and linewidth enhancement factor α_g (α_q) in the gain (absorber) section of the laser. The parameter scans were performed by taking a stable LB calculated at fixed values of the linewidth enhancement factors $\alpha_g = 1.5$ and $\alpha_q = 0.5$ as an initial condition, and then performing numerical continuation of the LB branch by increasing and decreasing g_0. For each value of g_0, $N = 100$ round-trips in the laser cavity were calculated. After that we calculate the center of the stability range in g_0, pick the corresponding LB as an initial condition, make a small
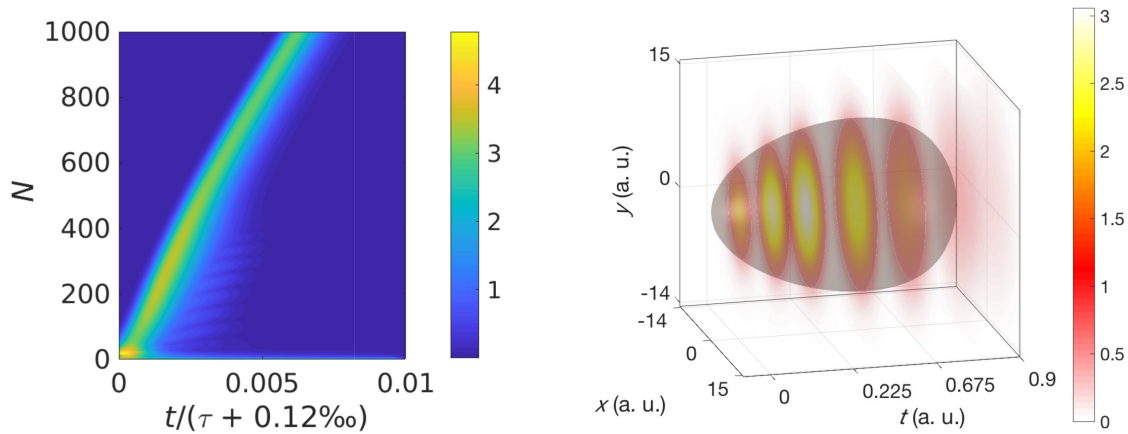
Figure 3: Three-dimensional LB obtained by numerical solution of Eqs. (4)-(6) for $g_0 = 0.69$. Left panel demonstrates the space-time representation of the maximal intensity $\max_x |A(t, x, y)|^2$, whereas right panel shows a spatiotemporal profile of the LB intensity $|A(t, x, y)|^2$. Other parameters are as in Fig. 2.

step in the linewidth enhancement factor, and repeat the above described procedure. It is noteworthy that the stability domains shown in Fig. 4 are in very good qualitative agreement with those obtained in [8] using the Haus-type model. It can be seen from this figure that moderate nonzero linewidth enhancement factors can enlarge the LB stability range. The main difference of the results presented here with those obtained using the Haus-type model is that in the NDDE system (5)-(7) predicts slightly larger stability domains of LBs. We suggest that this discrepancy may be attributed to finite size of the integration interval, different continuation procedures, as well as to the use of different models. Note that the lack of quantitative agreement between the results reported in [8] with the bifurcation diagrams shown in Fig. 4 may indicate that future studies could profit from the use of NDDE models even in the parameter domain where MF Haus-type mode-locking models were successfully applied earlier for qualitative analysis of the LB formation [7, 8]. More detailed comparison of the two models requires further studies.

4.2   Light bullets beyond the MF approximation

In the previous subsection we demonstrated that in the MF limit the results obtained with the NDDE models (4)-(7) are in a very good agreement with those from the Haus-type model used in [7, 8], and pointed out some minor discrepancies between the two models. In this subsection we use the NDDE model to investigate how the properties of LBs are modified away from the MF limit. To this end we consider relatively large gain and loss per cavity round trip time, which is typical of semiconductor lasers: $\kappa = 0.3$, $Q_0 = 2.0$, $\gamma_g = 0.04$, $\gamma_q = 1.0$, $s = 30$, $\gamma = 10$, $T = 200$, $\alpha_g = 1.5$, $\alpha_q = 0.5$. A stable two-dimensional LB obtained by numerical integration of Eqs. (5)-(7) with $g_0 = 0.83$ is presented in Fig. 5. Using two-parameter scan similar to that described in the previous subsection, we find even larger parameter domains of the existence of stable LBs than those obtained in the case of relatively small gain and loss, compare Fig. 6 with Fig. 4. Note, that when the difference $\alpha_g - \alpha_q$ becomes sufficiently large (between 1.5 and 2, see, e.g., the region $0 \leq \alpha_q \leq 0.2$ in the right panel of Fig. 6), a sufficiently good initial guess is required to ensure a convergence of the solution to a stable LB. Finally, Fig. 7 shows an example of stable three-dimensional LB obtained by solving Eqs (4)-(6) with $g_0 = 0.92$.
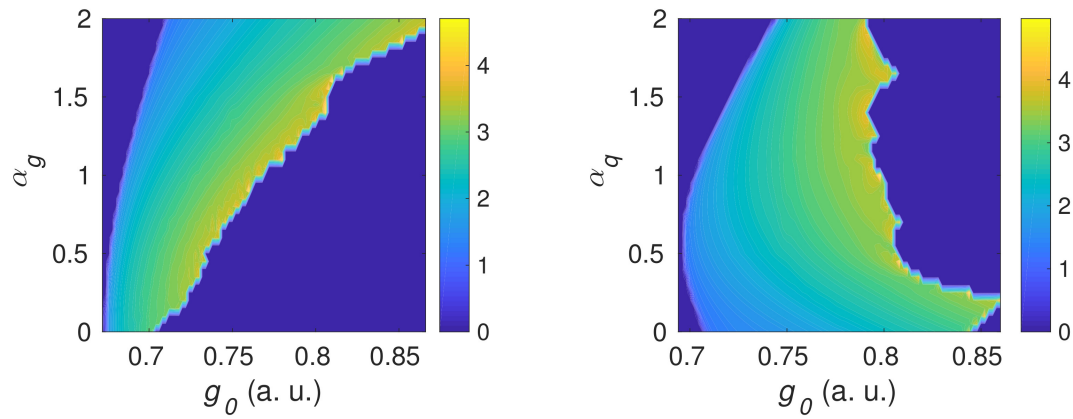
Figure 4: Domains of the existence of stable two-dimensional LBs calculated by numerical integration of Eqs. (5)-(7). Left (right) panel is obtained by varying the parameters g_0 and α_g (α_q) with fixed $\alpha_q = 0.5$ ($\alpha_g = 1.5$). Other parameters are as in Fig. 2. The color code represents the peak intensity of the LB pulse.
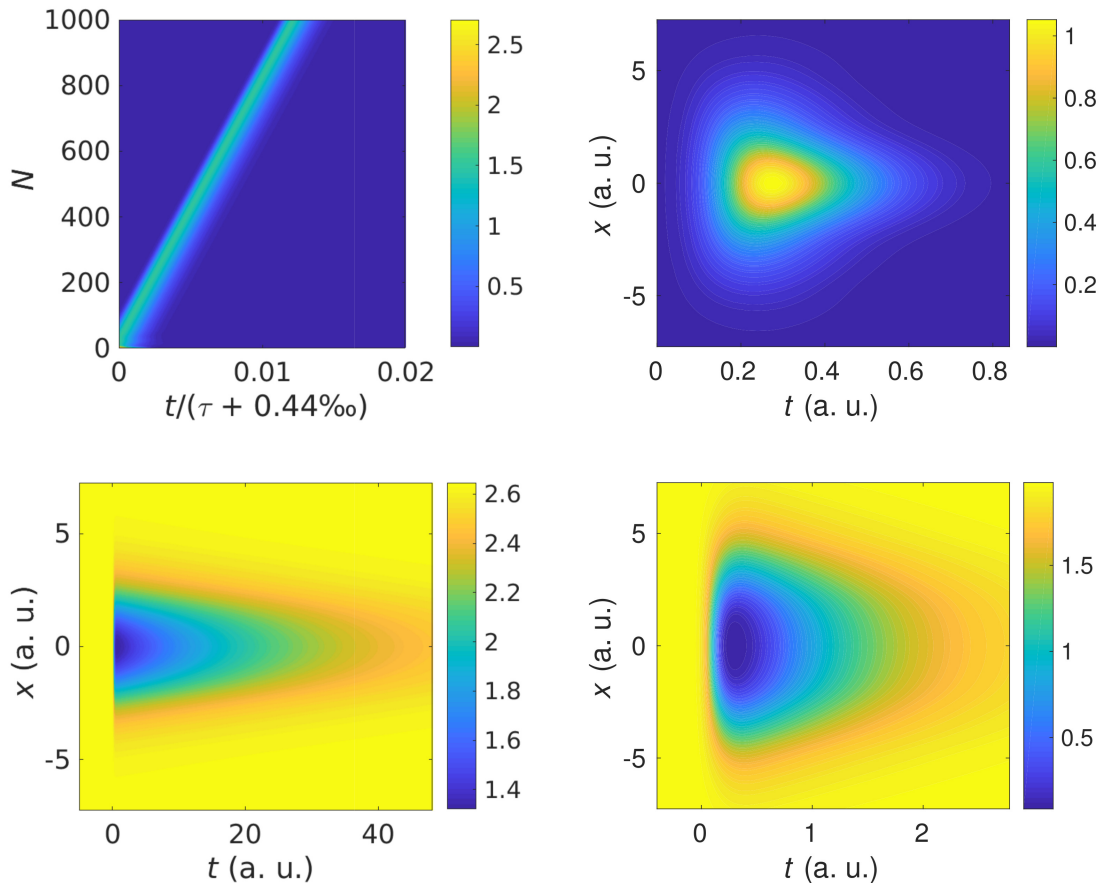
Figure 5: Two-dimensional LB obtained by the numerical integration of Eqs. (5)-(7) for $g_0 = 0.83$. Top left panel demonstrates space-time representation of the maximal intensity $\max_x |A(t,x)|^2$. Top right, bottom left and right panels show spatiotemporal profiles of the LB intensity $|A(t,x)|^2$, saturable gain $G(t,x)$, and saturable absorption $Q(t,x)$, correspondingly. Other parameters are: $\kappa = 0.3$, $q_0 = 2.0$, $\gamma_g = 0.04$, $\gamma_q = 1.0$, $s = 30$, $\gamma = 10$, $T = 200$, $\alpha_g = 1.5$, $\alpha_q = 0.5$.
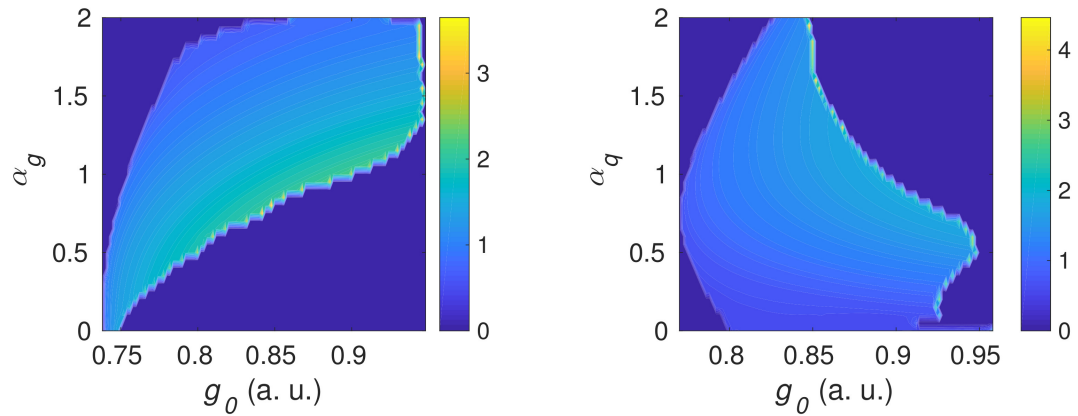
Figure 6: Domains of existence of stable LBs obtained by numerical integration of Eqs. (5)-(7). Left (right) panel is obtained by varying two parameters g_0 and α_g (α_q) with fixed $\alpha_q = 0.5$ ($\alpha_g = 1.5$). Other parameters are as in Fig. 5. The color code represents the peak intensity of the LB pulse.
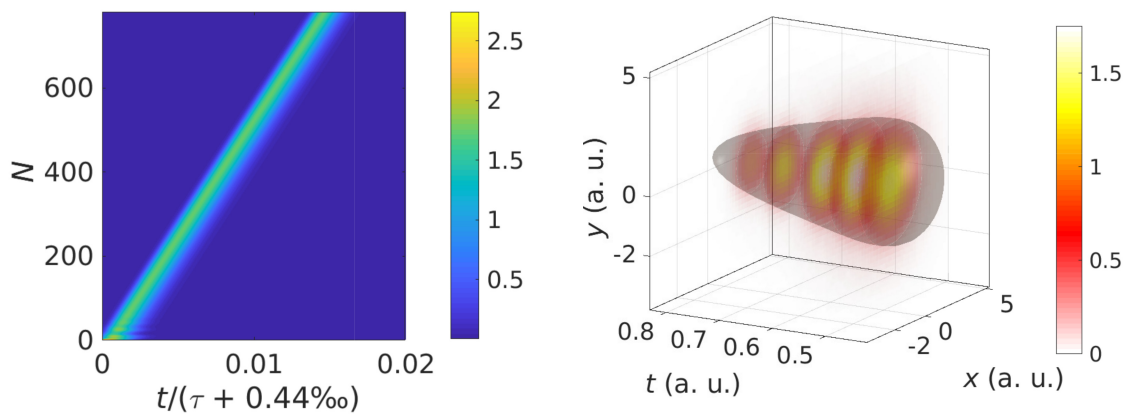
Figure 7: Three-dimensional LB obtained by the numerical solution of Eqs. (4)-(6) for $g_0 = 0.92$. Other parameters are as in Fig. 5. Left panel demonstrates space-time representation of the maximal intensity $\max_x |A(t, x, y)|^2$. Right panel shows spatiotemporal profile of the LB intensity $|A(t, x, y)|^2$.
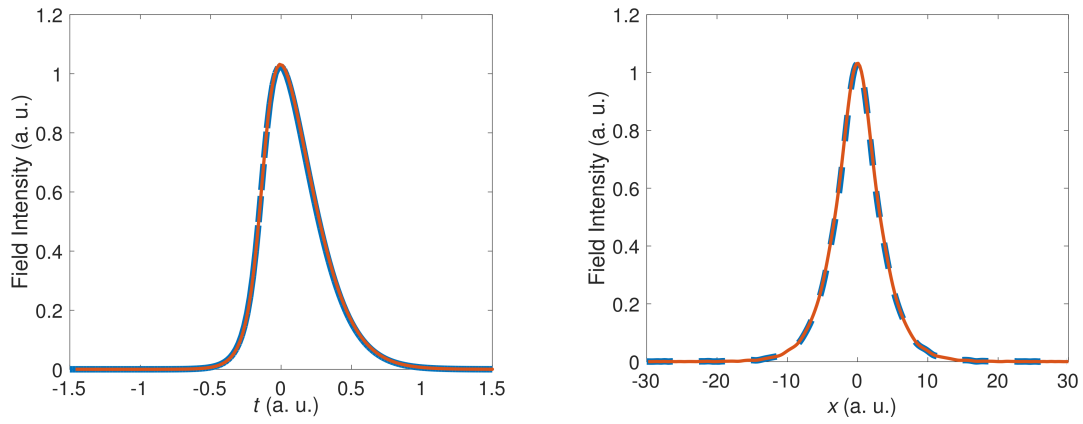
Figure 8: Longitudinal (left) and transverse (right) intensity profiles of two-dimensional LBs obtained by direct numerical integration of Eqs. (5-7) and using the functional mapping (12) are shown by dashed blue line and solid red line, respectively. Parameters are the same as in Fig. 5.

4.3   Spectral method

As we have already mentioned above, the application of spectral method based on the functional mapping described in subsection 3.2 allows to calculate LB solution on a time interval much shorter than the cavity round trip time T and, hence, to reduce considerably the amount of calculations. Transverse and longitudinal profiles of two-dimensional LB solution calculated with the help of the optimized spectral method given by Eq. (12) are presented in Fig. 8 together with the profiles obtained by direct numerical solution of the NDDE model (4)-(6) using the method described in subsection 3.1. One can see that the agreement between the results obtained with two different numerical approaches is almost perfect. Similarly, the stability domains of LB solution calculated with the help of the functional mapping method and shown in Fig. 9 are in a good agreement with those presented in Fig. 6. Small discrepancies in the two-parameter stability diagrams can be explained by differences in numerical continuation procedure. In particular, the continuation of the LB solution can be performed only with a good initial guess, which we accomplished as described in the previous subsection. On the other hand, numerical simulations of the mapping procedure (12) are very fast, and it is more efficient to perform two-parameter scans by finding a stable LB solution for each value of the linewidth enhancement factor and then continuing it in g_0. It is seen from Fig. 9 that the latter approach fails to find a stable LBs around $\alpha_g \approx 2$ (see left panel of Fig. 9) and $\alpha_q \approx 0.2$ (see right panel of Fig. 9), whereas slower continuation approach based on direct numerical integration of Eqs. (5-7) indicates that stable LBs exist in these parameter domains (cf. Fig. 6). This discrepancy is related to the fact that at large differences $\alpha_g - \alpha_q$ it is hardly possible to excite stable LBs from arbitrary initial condition not only by using the functional mapping method, but also by solving numerically the NDDE system on the full round trip time interval.

Finally, we use the functional mapping (12) to investigate the effect of large losses on the LB stability domain. Figure 10 illustrates how the stability domain on the plane of two parameters, normalized unsaturated gain g_0, and normalized unsaturated loss $q_0 = \frac{Q_0}{-\log \kappa}$, changes with the decrease of the linear attenuation factor κ, i.e. with the increase of the linear cavity losses. Note that similar bifurcation diagram reported in [8] for the case small losses, $\kappa = 0.8$, is qualitatively similar to that shown in Fig. 10. It follows also from this figure that the LB stability range increases with the absolute value of the unsaturated loss parameter. The LB stability domains on the plane of two parameters, normalized
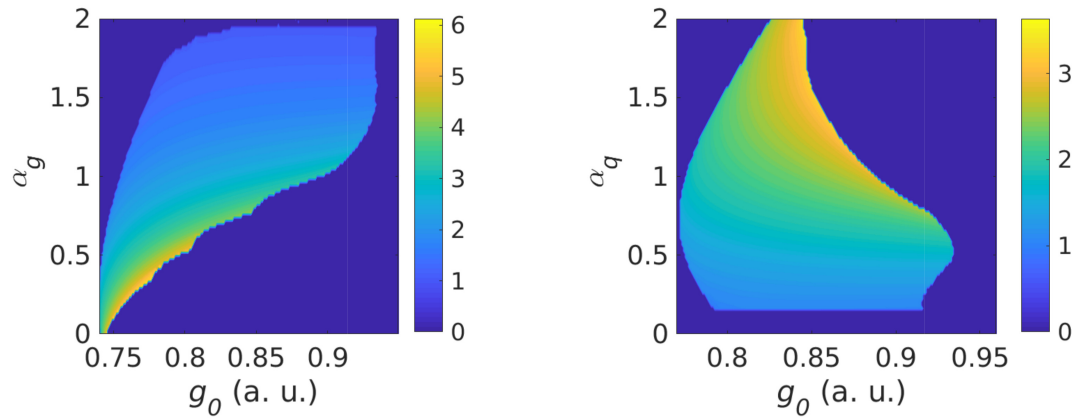
Figure 9: Domains of existence of stable two-dimensional LBs obtained with the help of the functional mapping (12). Left (right) panel is obtained by varying the parameters g_0 and α_g (α_q) with fixed $\alpha_q = 0.5$ ($\alpha_g = 1.5$). Other parameters are as in Fig. 5. Color code represents the energy of the pulse, $\iint |A(t,x)|^2 dx dt$.

pump parameter g_0, and attenuation factor κ, are shown in the left panel of Fig. 11 corresponding to fixed value of the unsaturated absorption parameter $Q_0 = 1$. According to this figure the increase of linear losses results in a slight decrease of the LS stability range. Finally, by decreasing κ and increasing Q_0 so that $q_0 = \frac{Q_0}{-\log \kappa} = 1$ is constant, we see from right panel of Fig. 11 that the decrease of the LS stability range due to increased losses can be compensated by increasing the unsaturated loss parameter. Furthermore, by increasing κ up to 0.99 and decreasing Q_0 simultaneously we see that the LB broadens in all dimensions, and in the regime, when the linear and saturable losses are small enough and the length of the LB becomes larger than the absorber recovery time, $\gamma_q^{-1} = 1$, we observe that the LB stability range in g_0 shrinks fast to the point $g_0 = \kappa = 1$ corresponding to the MF limit with a fast absorber.

5   Conclusion

We have proposed a NDDE model of a wide-aperture mode-locked laser and used this model to demonstrate the existence of stable LBs in a semiconductor lasers where the small gain and loss approximation is hardly justified. Unlike the Haus-type model, which was used previously to predict the existence of LBs and explain the mechanism of their formation theoretically [7, 8], the NDDE model is not based on the MF approximation. We have shown that in the MF approximation the qualitative agreement between the results obtained using these two models is very good. An interesting question, how far the agreement between NDDE and Haus-type models regarding the existence and the stability properties of the LBs stands, could be a subject of further studies. For example, it is known that the Q-switching instability of the mode-locked regime is well described by the DDE model, but can be missing in Haus-type models [28]. Moving away from the MF approximation we have demonstrated the existence of LBs in a laser with relatively large gain and losses per cavity round trip. We have found that the increase of the absolute value of the unsaturated loss parameter can lead to an increase of the stability range of LBs, and, in particular, to a compensation of the destabilizing effect of large linear losses. Thus, our results provide further guidelines for future experimental observation of LBs in mode-locked semiconductor lasers.
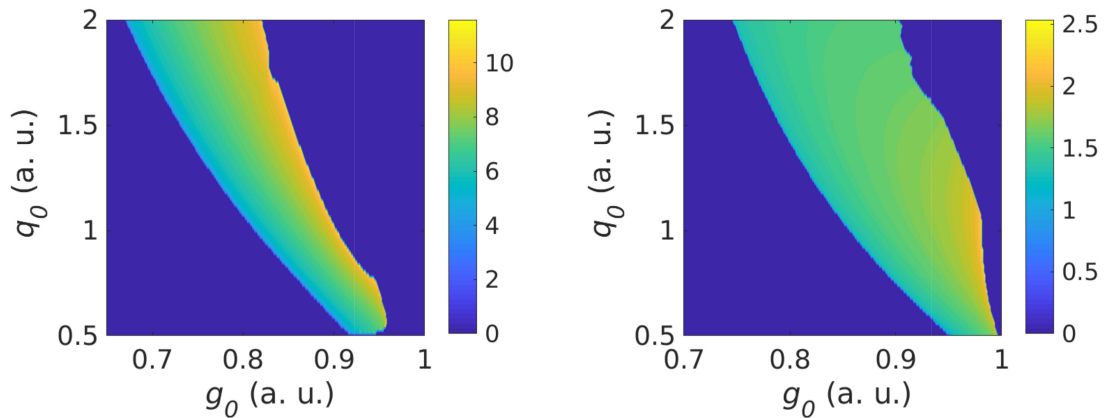
Figure 10: Domains of existence of stable LBs on the plane of two parameters, g_0 and $q_0 = \frac{Q_0}{-\log \kappa}$, obtained with the help of the functional mapping (12). Left (right) panel corresponds to $\kappa = 0.8$ ($\kappa = 0.3$). Other parameters are as in Fig. 5. Color code represents the energy of the pulse.
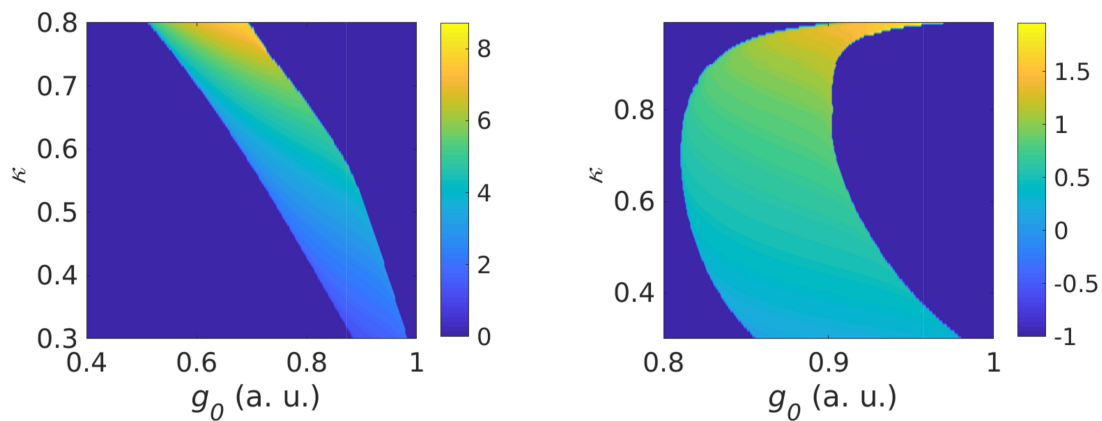
Figure 11: Domains of existence of stable LBs obtained with the help of the functional mapping (12) by varying the parameters g_0 and κ with fixed $Q_0 = 1$ (left) and with varying $Q_0 = -\log \kappa$ (i.e., fixed $q_0 = 1$) (right). Other parameters are as in Fig. 5. Color code represents the energy of the pulse.

References

[1] Yaron Silberberg. Collapse of optical pulses. *Optics letters*, 15(22):1282–1284, 1990.

[2] V. E. Zakharov. Collapse of Langmuir waves. *Soviet Physics JETP*, 35(5):908–914, 1972.

[3] J. J. Rasmussen and K. Rypdal. Blow-up in nonlinear Schroedinger equations-I. A general review. *Physica Scripta*, 33:481–497, 1986.

[4] Nikolay Veretenov and Mustapha Tlidi. Dissipative light bullets in an optical parametric oscillator. *Phys. Rev. A*, 80:023822, Aug 2009.

[5] N.A. Veretenov, A.G. Vladimirov, N.A. Kaliteevskii, N.N. Rozanov, S.V. Fedorov, and A.N. Shatsev. Conditions for the existence of laser bullets. *Optics and Spectroscopy*, 89(3):380–383, 2000.

[6] M. Brambilla, T. Maggipinto, G. Patera, and L. Columbo. Cavity light bullets: Three-dimensional localized structures in a nonlinear optical resonator. *Phys. Rev. Lett.*, 93:203901, 2004.

[7] J. Javaloyes. Cavity light bullets in passively mode-locked semiconductor lasers. *Phys. Rev. Lett.*, 116:043901, Jan 2016.

[8] S. V. Gurevich and J. Javaloyes. Spatial instabilities of light bullets in passively-mode-locked lasers. *Phys. Rev. A*, 96:023821, Aug 2017.

[9] A. G. Vladimirov and D. Turaev. New model for mode-locking in semiconductor lasers. *Radiophys. & Quant. Electron.*, 47(10-11):857–865, 2004.

[10] A. G. Vladimirov and D. Turaev. Model for passive mode-locking in semiconductor lasers. *Phys. Rev. A*, 72:033808 (13 pages), 2005.

[11] A.G. Vladimirov, D. Turaev, and G. Kozyreff. Delay differential equations for mode-locked semiconductor lasers. *Opt. Lett.*, 29:1221–1223, 2004.

[12] Mathias Marconi, Julien Javaloyes, Salvador Balle, and Massimo Giudici. How lasing localized structures evolve out of passive mode locking. *Phys. Rev. Lett.*, 112(22):223901, 2014.

[13] D. Puzyrev, A. G. Vladimirov, A. Pimenov, S. V. Gurevich, and S. Yanchuk. Bound pulse trains in arrays of coupled spatially extended dynamical systems. *Phys. Rev. Lett.*, 119:163901, Oct 2017.

[14] M. Heuck, S. Blaaberg, and J. Mørk. Theory of passively mode-locked photonic crystal semiconductor lasers. *Opt. Express*, 18(17):18003–18014, 2010.

[15] A. Pimenov, V. Z. Tronciu, U. Bandelow, and A. G. Vladimirov. Dynamical regimes of a multistripe laser array with external off-axis feedback. *J. Opt. Soc. Am. B*, 30(6):1606–1613, Jun 2013.

[16] S. Slepneva, B. Kelleher, B. O'Shaughnessy, S.P. Hegarty, A. G. Vladimirov, and G. Huyet. Dynamics of fourier domain mode-locked lasers. *Opt. Express*, 21(16):19240–19251, 2013.

[17] S. Slepneva, B. O'Shaughnessy, B. Kelleher, S.P. Hegarty, A. G. Vladimirov, H.C. Lyu, K. Karnowski, M. Wojtkowski, and G. Huyet. Dynamics of a short cavity swept source oct laser. *Opt. Express*, 22(15):18177–18185, 2014.

[18] Lina Jaurigue, Alexander Pimenov, Dmitrii Rachinskii, Eckehard Schöll, Kathy Lüdge, and Andrei G. Vladimirov. Timing jitter of passively-mode-locked semiconductor lasers subject to optical feedback: A semi-analytic approach. *Phys. Rev. A*, 92:053807, Nov 2015.

[19] N. Rebrova, G. Huyet, D. Rachinskii, and A. G. Vladimirov. Optically injected mode-locked laser. *Physical Review E*, 83:066202, 2011.

[20] R. Arkhipov, A. Pimenov, M. Radziunas, D. Rachinskii, A. G. Vladimirov, D. Bimberg, and et al. Hybrid mode-locking in semiconductor lasers: simulations, analysis and experiments. *IEEE Jornal of Selected Topics in QE*, 99:1100208, 2013.

[21] A. Pimenov, E. A. Viktorov, S. P. Hegarty, T. Habruseva, G. Huyet, D. Rachinskii, and A. G. Vladimirov. Bistability and hysteresis in an optically injected two-section semiconductor laser. *Phys. Rev. E*, 89:052903, May 2014.

[22] R. M. Arkhipov, T. Habruseva, A. Pimenov, M. Radziunas, S. P. Hegarty, G. Huyet, and A. G. Vladimirov. Semiconductor mode-locked lasers with coherent dual-mode optical injection: simulations, analysis, and experiment. *J. Opt. Soc. Am. B*, 33(3):351–359, Mar 2016.

[23] Y. L. Wong and J. E. Carroll. A travelling-wave rate equation analysis for semiconductor lasers. *Solid-State Electronics*, 30(1):13–19, 1987.

[24] U. Bandelow, M. Radziunas, J. Sieber, and M. Wolfrum. Impact of gain dispersion on the spatio-temporal dynamics of multisection lasers. *IEEE Journal of Quantum Electronics*, 37(2):183–188, 2001.

[25] U. Bandelow, M. Radziunas, A.G. Vladimirov, B. Huettl, and R. Kaiser. 40 GHz modelocked semiconductor lasers: Theory, simulations and experiment. *Optical and Quantum Electronics*, 38(4-6):495–512, 2006.

[26] J. Javaloyes and S. Balle. Mode-locking in semiconductor fabry-perot lasers. *Quantum Electronics, IEEE Journal of*, 46(7):1023 –1030, july 2010.

[27] J. Javaloyes and S. Balle. Quasiequilibrium time-domain susceptibility of semiconductor quantum wells. *Phys. Rev. A*, 81:062505, Jun 2010.

[28] Theodore Kolokolnikov, Michel Nizette, Thomas Erneux, Nicolas Joly, and Serge Bielawski. The Q-switching instability in passively mode-locked lasers. *Physica D: Nonlinear Phenomena*, 219(1):13–21, 2006.

[29] A. G. Vladimirov, G. Huyet, and A. Pimenov. Delay differential models in multimode laser dynamics: taking chromatic dispersion into account. *Proc. SPIE*, 9892:98920I–98920I–7, 2016.

[30] Alexander Pimenov, Svetlana Slepneva, Guillaume Huyet, and Andrei G. Vladimirov. Dispersive time-delay dynamical systems. *Phys. Rev. Lett.*, 118:193901, May 2017.

[31] Mustapha Tlidi, AG Vladimirov, Didier Pieroux, and Dmitry Turaev. Spontaneous motion of cavity solitons induced by a delayed feedback. *Physical review letters*, 103(10):103904, 2009.

[32] Krassimir Panajotov and Mustapha Tlidi. Spontaneous motion of cavity solitons in vertical-cavity lasers subject to optical injection and to delayed feedback. *The European Physical Journal D-Atomic, Molecular, Optical and Plasma Physics*, 59(1):67–72, 2010.

[33] Alexander Pimenov, Andrei G Vladimirov, Svetlana V Gurevich, Krassimir Panajotov, Guillaume Huyet, and Mustapha Tlidi. Delayed feedback control of self-mobile cavity solitons. *Physical Review A*, 88(5):053830, 2013.

[34] Dmitry Puzyrev, Serhiy Yanchuk, AG Vladimirov, and SV Gurevich. Stability of plane wave solutions in complex ginzburg–landau equation with delayed feedback. *SIAM Journal on Applied Dynamical Systems*, 13(2):986–1009, 2014.

[35] Giovanni Giacomelli and Antonio Politi. Relationship between delayed and spatially extended dynamical systems. *Phys. Rev. Lett.*, 76:2686–2689, Apr 1996.